Human Hypertension Caused by Mutations in WNK Kinases

Frederick H. Wilson,[1] Sandra Disse-Nicodème,[2]* Keith A. Choate,[1]* Kazuhiko Ishikawa,[1]* Carol Nelson-Williams,[1] Isabelle Desitter,[2] Murat Gunel,[1] David V. Milford,[3] Graham W. Lipkin,[4] Jean-Michel Achard,[5] Morgan P. Feely,[6] Bertrand Dussol,[7] Yvon Berland,[7] Robert J. Unwin,[8] Haim Mayan,[9] David B. Simon,[1] Zvi Farfel,[9] Xavier Jeunemaitre,[2] Richard P. Lifton[1]†

Hypertension is a major public health problem of largely unknown cause. Here, we identify two genes causing pseudohypoaldosteronism type II, a Mendelian trait featuring hypertension, increased renal salt reabsorption, and impaired K^+ and H^+ excretion. Both genes encode members of the WNK family of serine-threonine kinases. Disease-causing mutations in *WNK1* are large intronic deletions that increase *WNK1* expression. The mutations in *WNK4* are missense, which cluster in a short, highly conserved segment of the encoded protein. Both proteins localize to the distal nephron, a kidney segment involved in salt, K^+, and pH homeostasis. WNK1 is cytoplasmic, whereas WNK4 localizes to tight junctions. The WNK kinases and their associated signaling pathway(s) may offer new targets for the development of antihypertensive drugs.

High blood pressure or hypertension affects 25% of most adult populations and is an important risk factor for death from stroke, myocardial infarction, congestive heart failure, and renal failure (*1*). The molecular pathogenesis of the most common forms of hypertension is poorly understood. The study of rare Mendelian forms of high and low blood pressure may provide important clues to the pathways underlying more common forms of disease and may identify targets and pathways for new approaches to treatment (*2*). Pseudohypoaldosteronism type II (PHAII; Online Mendelian Inheritance in Man #145260) is an autosomal dominant disorder in which patients present with hypertension and hyperkalemia (high serum potassium level). The hypertension has been attributed to increased renal salt reabsorption and the hyperkalemia to reduced renal K^+ excretion, despite normal glomerular filtration and aldosterone secretion; reduced renal H^+ secretion is also commonly seen, resulting in metabolic acidosis (*3, 4*). The features of PHAII are chloride-dependent, because they are corrected when infusion of sodium sulfate or sodium bicarbonate is substituted for sodium chloride (*5, 6*); in addition, these abnormalities are ameliorated by thiazide diuretics (*4*), which inhibit salt reabsorption in the distal nephron. Together, the features of PHAII point to a primary defect in renal electrolyte handling, but are not readily explained by known physiologic mechanisms. Genes for PHAII have been mapped in different families to chromosome 17, 1, or 12 (*7, 8*), but no compelling candidate genes have been identified.

We have studied a new PHAII kindred, K22 (*9*). This kindred includes 10 living members with typical features of PHAII including hypertension (blood pressure >140/90 mm Hg in adults), hyperkalemia (mean serum K^+ of 6.2 mM; normal is 3.5 to 5.0), normal glomerular filtration rate, suppressed plasma renin activity, normal or elevated aldosterone levels, hyperchloremia (mean serum Cl^- of 112 mM; normal is 95 to 105), and reduced bicarbonate (mean serum bicarbonate of 17.5 mM; normal is 22 to 28). These features were absent in unaffected kindred members. Inheritance of the trait was consistent with autosomal dominant transmission with high penetrance (Fig. 1A). Genome-wide analysis of linkage (*10*) demonstrated complete linkage of PHAII to the most telomeric 2-centimorgan (cM) segment of chromosome 12p, with a multipoint lod score of 5.07 (odds ratio greater than 10^5:1 in favor of linkage) (Fig. 1, A and B).

A deletion in the linked interval. Additional loci in the completely linked telomeric interval were genotyped. One of these, *D12S94*, violated simple Mendelian transmission: all affected members were apparent homozygotes at this locus, and in all four informative matings, affected offspring inherited no allele from their affected parent (Fig. 1A). This finding indicates a null allele, consistent with a deletion within the disease-linked chromosome segment.

Genomic sequence of the interval containing this marker permitted identification of three additional polymorphic loci in close proximity to *D12S94* (*11*) (Fig. 2A). Genotyping of these loci in K22 provided evidence of a null allele for each on the disease chromosome, with no evidence of transmission of alleles from affected parents to affected offspring (Fig. 1A). Flanking loci *D12S341* and *D12S91* showed no violations of Mendelian transmission. These findings indicate a deletion in the interval between *D12S341* and *D12S91*.

We next determined endpoints of this deletion by Southern blotting of genomic DNA from kindred members, using the genomic sequence of the interval to define probes and restriction enzyme cleavage fragments for systematic screening (Fig. 2A) (*12*). A novel 6.9-kb fragment on the disease-linked chromosome was detected with two probes that are widely separated in wild-type genomic DNA (Fig. 2B). This result is consistent with a large deletion that encompasses the four loci showing null alleles by linkage (Fig. 2A).

Polymerase chain reaction (PCR) was used to amplify a product that spans the deletion endpoints (*13*). A primer pair normally separated by 42 kb in genomic DNA yielded a novel 600–base pair (bp) fragment when genomic DNA of affected, but not unaffected kindred members or 160 unrelated controls, was used as template (Fig. 2C). The DNA sequence of this fragment indicates that it arises from a deletion of 41, 241 bp from normal genomic DNA (Fig. 2C). The two deletion endpoints occur within Alu repetitive elements (Fig. 2C). Use of other primer pairs confirms the presence of this deletion (*14*). Thus, a novel 41 kb genomic deletion cosegregates with PHAII in K22.

PHAII deletions lie in intron 1 of *WNK1* and increase its expression. Analysis of genomic sequence (*15*) revealed that the deletion lies within the large first intron of the human ortholog of rat *WNK1*, a recently described serine-threonine kinase (*16*). This kinase is distinctive in having cysteine instead of lysine at a key position in the active site, and also contains two putative coiled-coil domains. The *hWNK1* gene is encoded in 28 exons that span 156 kb in genomic DNA (Fig. 2D) and the encoded human and rat proteins are 86% identical in amino acid sequence. Transcripts of *hWNK1* are found in

[1]Howard Hughes Medical Institute; Yale University School of Medicine, Boyer Center for Molecular Medicine, 295 Congress Avenue, New Haven, CT 06510 USA. [2]INSERM U36, Collège de France. 11, Place Marcellin Berthelot. 75005 Paris, France. [3]Department of Nephrology, Birmingham Children's Hospital, Birmingham B4 6NH, UK. [4]Department of Nephrology, Queen Elizabeth Hospital, Birmingham B15 2TH, UK. [5]Service de Néphrologie, Hopital d'Amiens-Sud, Amiens, France. [6]Unit of Molecular Vascular Medicine, The General Infirmary, Leeds, UK. [7]Service de Néphrologie et Hémodialyse, Hopital Sainte Marguerite, Marseille, France. [8]Departments of Nephrology and Physiology, University College London, London W1W 7EY, UK. [9]Department of Medicine E' and Laboratory of Biochemical Pharmacology, Sheba Medical Center, Tel Aviv University School of Medicine, Tel Hashomer 52621, Israel.

*These authors contributed equally to this work.
†To whom correspondence should be addressed. E-mail: richard.lifton@yale.edu

most tissues (*17*), with two predominant length isoforms (Fig. 2E); a 10-kb transcript is expressed at high levels in the kidney, and a 12-kb transcript is predominant in heart and skeletal muscle.

One other PHAII kindred, K4, has shown linkage to 12p (*8*). All affected members share a haplotype across the 18 cM telomeric segment. Genotyping of loci across intron 1 of *hWNK1* revealed null alleles for loci *STS45K* and *STS60K* (*14*). PCR using primers from this interval produced a novel 2.4-kb product, absent in 160 controls, that precisely cosegregated with PHAII in this kindred (Fig. 2F), and its DNA sequence revealed a deletion of 21,761 bp (Fig. 2F). The segment deleted in K4 is contained within the deleted segment of K22 (Fig. 2D). No deletions overlapping with this segment were detected in control subjects (*18*) and no mutations in the *hWNK1* coding sequence were detected in these or 16 other PHAII kindreds (*19*).

To determine if the PHAII-specific deletions alter the expression of *WNK1*, we compared *WNK1* transcript levels in leukocytes from three affected members of K4 and three unaffected individuals (two from K4 and one unrelated individual) (*20*). The affected individuals had a fivefold increase in the level of *hWNK1* transcripts (Fig. 2G), demonstrating that this intron 1 deletion alters *hWNK1* expression.

Mutations in *WNK4* on chromosome 17 also cause PHAII. Additional PHAII loci have been mapped to chromosomes 17 and 1 (*7*). We searched genomic sequence and EST databases for paralogs of *hWNK1* (*15*). Paralogs were identified on chromosomes 9 (*hWNK2*), X (*hWNK3*), and 17 (*hWNK4*). The encoded proteins all show high conservation in the kinase domain and have the distinctive substitution of cysteine for lysine in the active site (*14*). We localized *hWNK4* to the interval on chromosome 17 between loci *D17S250* and *D17S579*, both of which lie within the minimum genetic interval containing the *PHAIIB* locus on chromosome 17 (*7*). *hWNK4* is encoded in 19 exons contained within 16 kb of genomic DNA (*15*) (Fig. 3A). The encoded amino acid sequence of hWNK4 shows 76% identity to hWNK1 across a 370 amino acid segment spanning the kinase domain and the first putative coil domain, 51% identity across an 83 amino acid segment encompassing the COOH-terminal putative coil domain, and 52% identity across a 102 amino acid segment from residues 640 to 741 of WNK4 (Fig. 3B and Web fig. 1) (*21*). The intron-exon boundaries within these domains are conserved between the two genes (Web fig. 1) (*21*). *WNK4* is expressed virtually exclusively in the kidney (Fig. 3C) (*17*).

Examination of *WNK4* in PHAII kindreds (*19*) identified four missense mutations, all of which cosegregated with the disease (Fig. 4). Three of these are charge-changing substitutions that cluster in a span of four amino acids just distal to the first putative coil domain (Fig. 4, A through C). These all lie within a negatively charged 10 amino acid segment that is highly conserved among all members of the WNK family in human (Fig. 4F) as well as their known orthologs in mouse and rat (*22*). For example, in K13 (*23, 24*), a kindred previously linked to chromosome 17 (*7*), all eight affected members, but none of the unaffected members, inherit a single base substitution that produces a $Gln^{565} \rightarrow Glu$ substitution in WNK4 (Fig. 4, A and C). Similarly, mutations $Asp^{564} \rightarrow Ala$ and $Glu^{562} \rightarrow Lys$ were identified in affected members of K23 (*25*) and K11 (*26, 27*), respectively (Fig. 4, B and C). A fourth mutation, in PHAII kindred K21 (*28*), lies just distal to the second putative coil domain, and also changes charge, mutating $Arg^{1185} \rightarrow Cys$ at a residue conserved among WNK4, 1, and 2 (Fig. 4, D and E). None of these mutations were identified among 140 unrelated unaffected control subjects.

WNK1 and WNK4 localize to the distal nephron. To explore the expression patterns of WNK1 and WNK4, we prepared affinity-purified polyclonal antibodies that show specificity for each protein (Web fig. 2) (*21, 29*). Immunofluorescence microscopy of mouse kidney sections (*30*) demonstrated that both proteins localize to the distal convoluted

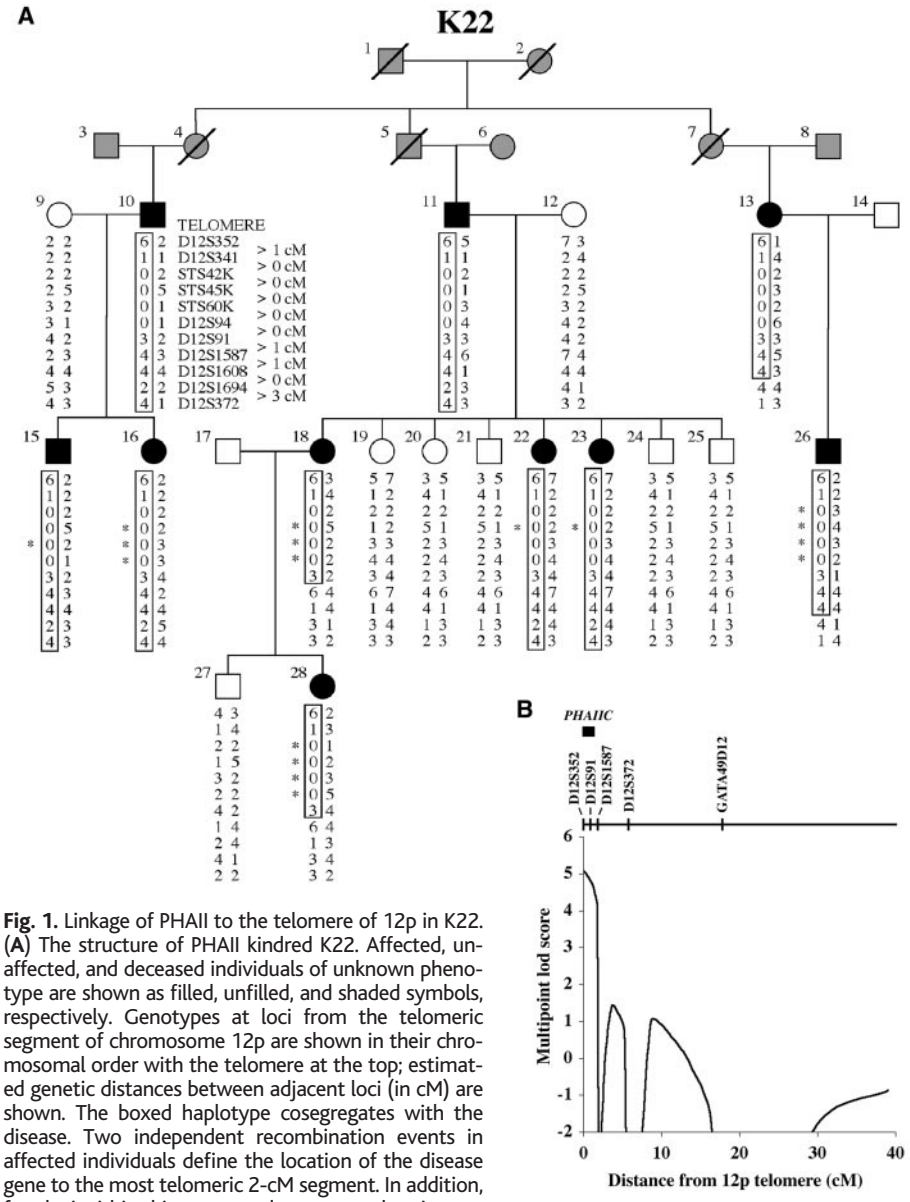

Fig. 1. Linkage of PHAII to the telomere of 12p in K22. (**A**) The structure of PHAII kindred K22. Affected, unaffected, and deceased individuals of unknown phenotype are shown as filled, unfilled, and shaded symbols, respectively. Genotypes at loci from the telomeric segment of chromosome 12p are shown in their chromosomal order with the telomere at the top; estimated genetic distances between adjacent loci (in cM) are shown. The boxed haplotype cosegregates with the disease. Two independent recombination events in affected individuals define the location of the disease gene to the most telomeric 2-cM segment. In addition, four loci within this segment demonstrate hemizygosity in affected kindred members; the inferred null alleles are denoted as "0." Genotypes that unambiguously demonstrate absence of transmission of an allele from affected parent to affected offspring are indicated by asterisks. (**B**) Multipoint lod score for linkage of PHAII to 12p in K22. The map of marker loci used in the multipoint analysis is shown at the top of the figure, and the 1000:1 support interval for the *PHAIIC* locus is indicated by the thick bar.

tubule (DCT) and the cortical collecting duct (CCD), adjacent segments of the distal nephron that play a key role in salt, water, K^+ and pH homeostasis (Figs. 5 and 6). WNK1 was also abundant in the medullary collecting duct; neither protein was detected elsewhere in the kidney (Web fig. 3) (*21*). WNK1 and WNK4 show distinct subcellular distribution patterns. WNK1 is present throughout the cytoplasm (Fig. 5) whereas WNK4 is present exclusively in intercellular junctions in the DCT and in both the cytoplasm and intercel-

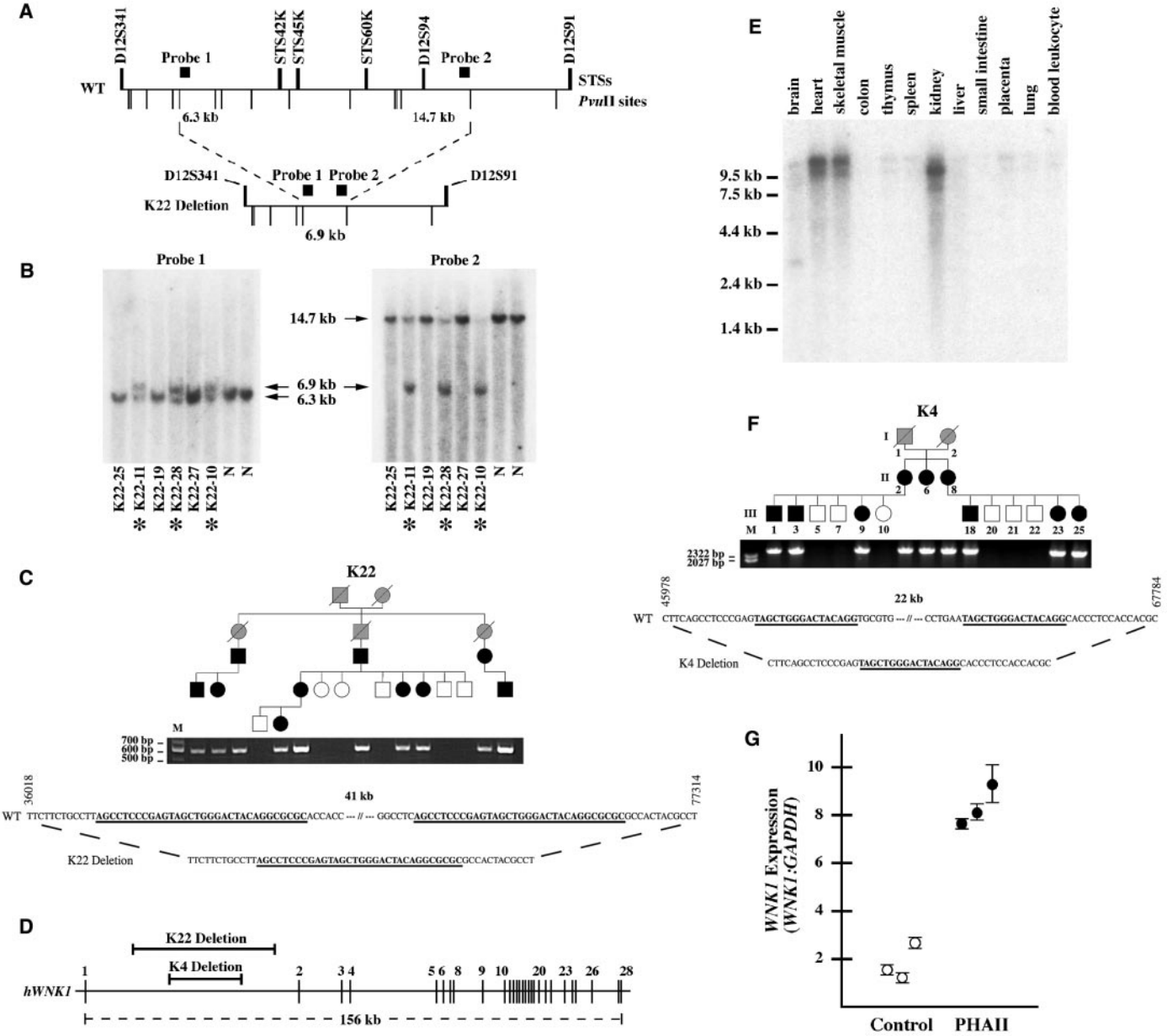

Fig. 2. Characterization of deletions in *WNK1* in PHAII. (**A**) Structure of wild-type (WT) and deleted alleles on 12p in K22 (*38*). Polymorphic sequence tagged sites (STSs) are indicated above the horizontal line representing genomic segments, and cleavage sites for *Pvu*II are indicated below. The locations of probes used for Southern blotting in (B) and the sizes of resulting fragments are indicated. (**B**) Identification of deletion endpoints by Southern blotting in K22. Southern blots hybridizing probes from (A) to genomic DNA digested with *Pvu*II are shown (*12*). Affected individuals of K22 are indicated by asterisks. (**C**) PCR across deletion endpoints in kindred K22. Products of PCR using primers separated by 42 kb in normal genomic DNA (*13*) are shown for members of K22 (M denotes marker lane); a 600-bp fragment cosegregates with PHAII. Below, the DNA sequence of a portion of the PCR product is compared to the sequence of the wild-type segment (WT). Numbered bases correspond to positions on the BAC clone in GenBank accession AC004765. The PCR product arises from a deletion whose endpoints fuse sequences normally separated by 41 kb. The deletion endpoints occur within a 32-bp repeated sequence (underlined). (**D**) Genomic structure of *hWNK1*. The genomic segment spanning *WNK1* is represented by a horizontal line, and exons are indicated by numbered vertical lines. The genomic segments that are deleted in K22 and K4 are indicated. (**E**) Northern blot of *hWNK1*. A probe from *hWNK1* was hybridized to RNA from a variety of human tissues (*17*). Locations of size standards in kilobases are indicated. (**F**) PCR across deletion endpoints in PHAII kindred K4. Primers separated by 24 kb in normal genomic DNA directed PCR from genomic DNA of members of K4; a 2.4-kb product cosegregates with PHAII. The DNA sequence demonstrated a 21.8-kb deletion, with the deletion endpoints in a 16-bp repeated sequence (underlined). (**G**) Increased levels of *hWNK1* transcripts in PHAII. Quantitative RT-PCR (*20*) was used to compare the levels of *hWNK1* and *GAPDH* transcripts in leukocytes from affected members of K4 (filled symbols) and control subjects (two unaffected members of K4 and one normal control subject; unfilled symbols). The mean and extreme values of repeated measures of the ratio of *WNK1*:*GAPDH* for each subject are shown.

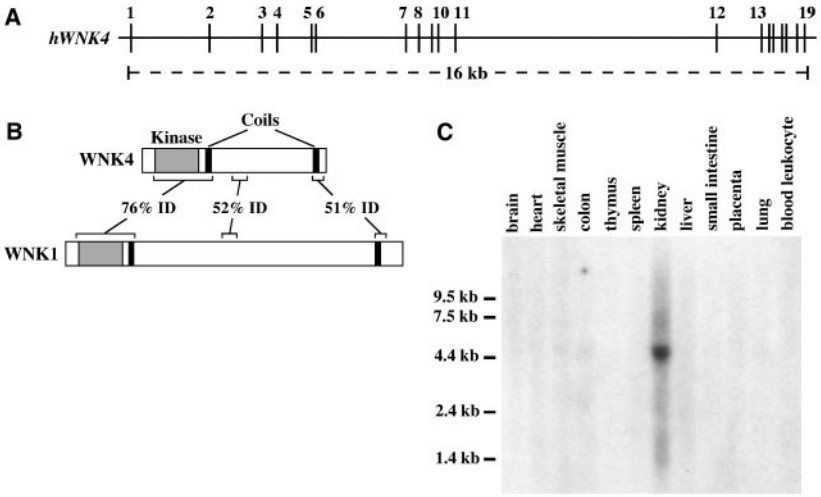

Fig. 3. Characterization of *hWNK4*. (**A**) Genomic structure of *hWNK4*. The genomic segment spanning *WNK4* is represented by a horizontal line, and exons of the gene are indicated by numbered vertical lines. (**B**) Comparison of hWNK1 and hWNK4. Domains of each protein are shown and the percentage amino acid identity (ID) between similar segments is indicated (*21*). Putative coil domains were predicted using the COILS program (*39*). (**C**) Northern blot of *hWNK4*. A probe from *hWNK4* was hybridized to RNA from a variety of human tissues (*17*). Locations of size standards in kilobases are indicated.

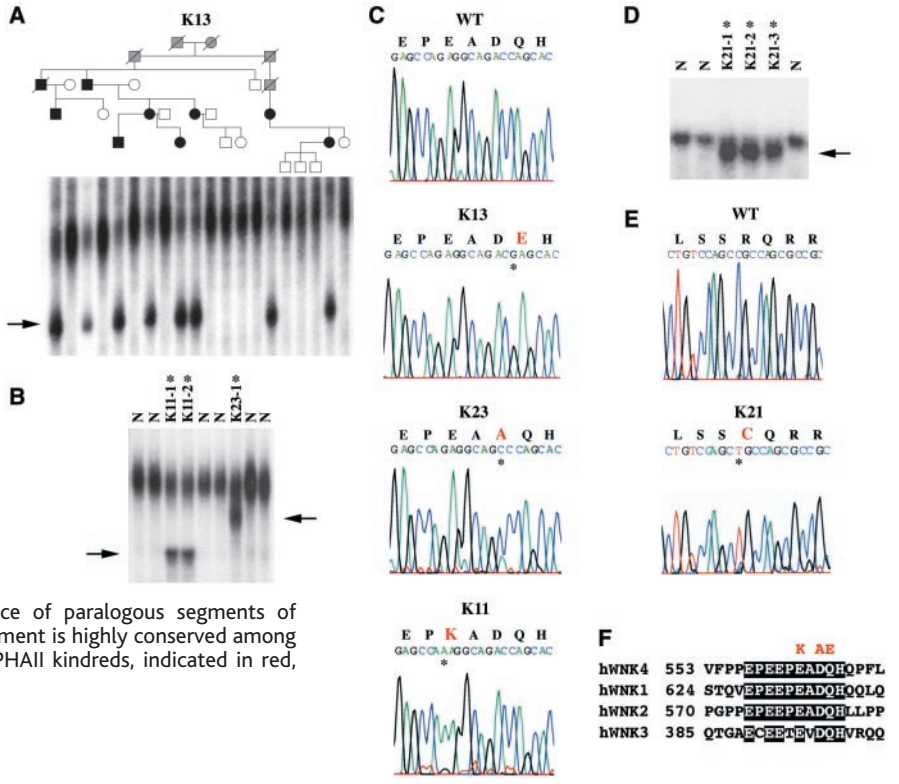

Fig. 4. Missense mutations in *hWNK4* in PHAII. (**A**) Mutation in exon 7 of *hWNK4* segregates with PHAII in K13. Products of SSCP from exon 7 are shown in members of K13 (*19*). A novel variant (indicated by arrow) cosegregates with PHAII. (**B**) Mutations in exon 7 of *hWNK4* in PHAII kindreds K11 and K23. Exon 7 was amplified as in (A). Affected members are indicated by asterisks and show novel variants (arrows) not seen in normal subjects (N). (**C**) DNA sequence of mutations in exon 7. The top panel shows the wild-type (WT) DNA sequence for codons 560 through 566 of *hWNK4*; the encoded amino acid sequence is shown above. In lower panels, the sequences of the variants identified in (A) and (B) are shown. Mutations are indicated by asterisks and the altered amino acids are shown in red. (**D**) Mutation in exon 17 in PHAII kindred K21. Exon 17 was amplified and fractionated as in panel A. The three affected members of K21 (asterisks) show a novel variant (arrow). (**E**) DNA sequence of mutation in exon 17. The WT DNA sequence for codons 1182 through 1188 of *hWNK4* is shown at the top, and the mutant sequence in K21 is shown below. (**F**) Conservation of residues mutated in PHAII among WNK family members. An 18 amino acid sequence of paralogous segments of hWNK1-4 is shown (*40*). An acidic 10 amino acid segment is highly conserved among all WNK family members. The mutations found in PHAII kindreds, indicated in red, alter completely conserved residues.

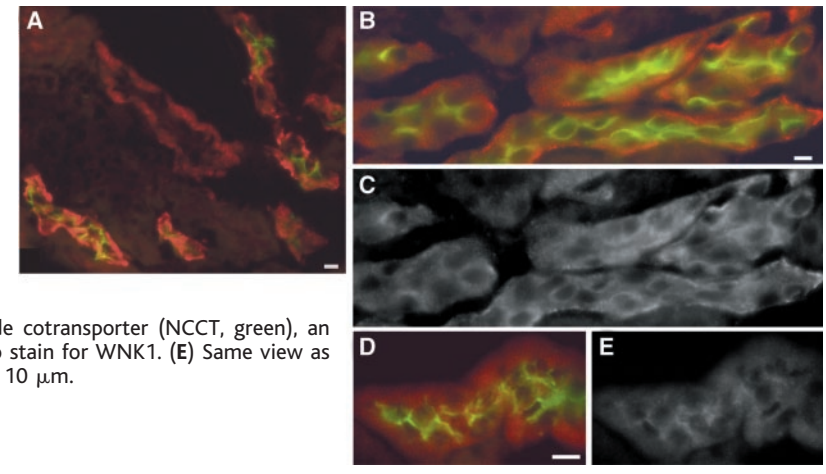

Fig. 5. Localization of WNK1 in kidney. Frozen mouse kidney sections were stained with antibodies and analyzed by fluorescence microscopy (*29, 30*). (**A**) Low-power view of renal cortex stained with anti-WNK1 (red) and anti–aquaporin-2 (AQP2, green), a marker of the connecting tubule and collecting duct. All tubules staining for AQP2 also stain for WNK1. In addition, other tubules in the cortex are also stained (DCT, see below). (**B**) Transverse section of cortical collecting duct (CCD) showing costaining with anti-WNK1 and anti-AQP2. (**C**) Same view as (B) showing only anti-WNK1 channel, and demonstrating cytoplasmic distribution of WNK1. (**D**) Transverse section of distal convoluted tubule (DCT) stained with anti-WNK1 (red) and antibody to the thiazide-sensitive sodium chloride cotransporter (NCCT, green), an apical marker of the DCT. All tubules staining for NCCT also stain for WNK1. (**E**) Same view as (D) showing only anti-WNK1 channel. White bars represent 10 μm.

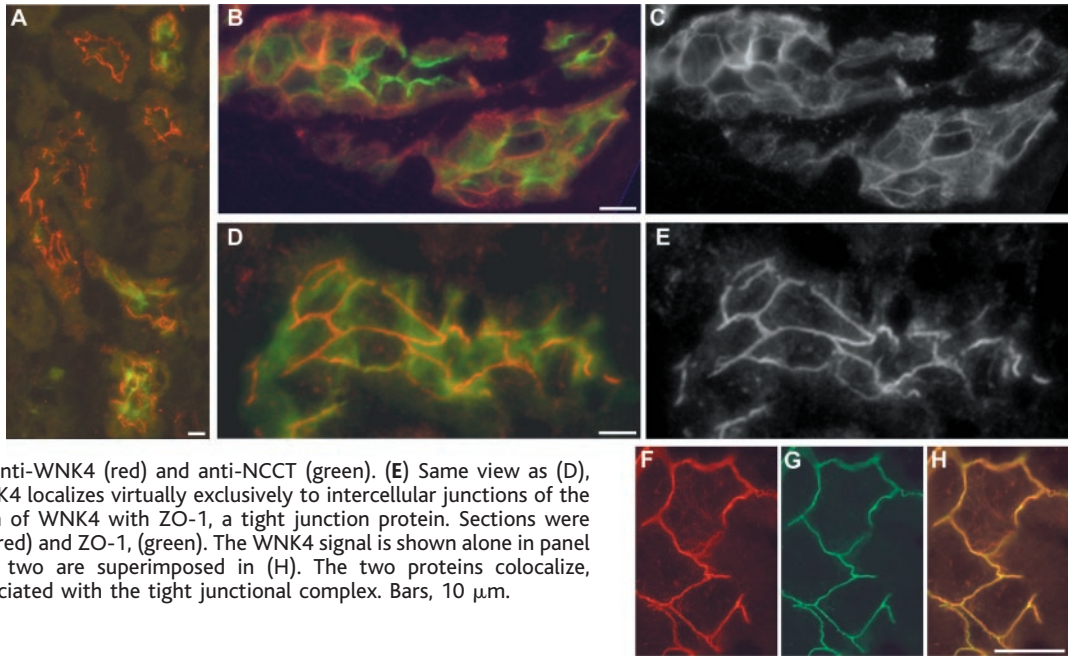

Fig. 6. Localization of WNK4 in kidney. Frozen mouse kidney sections were stained with antibodies as in Fig. 5. (**A**) Low-power view of renal cortex stained with anti-WNK4 (red) and anti-AQP2 (green). Segments staining for AQP2 also stain for WNK4; other tubules in the cortex (DCT, see below) are also stained by anti-WNK4. (**B**) Cortical collecting duct (CCD) shows staining with both anti-WNK4 and anti-AQP2. (**C**) Same view as (B), showing only the WNK4 staining. WNK4 localizes to both intercellular junctions and the cytoplasm in the CCD. (**D**) Distal convoluted tubule (DCT) shows staining with both anti-WNK4 (red) and anti-NCCT (green). (**E**) Same view as (D), showing only WNK4 staining. WNK4 localizes virtually exclusively to intercellular junctions of the DCT. (**F** through **H**) Colocalization of WNK4 with ZO-1, a tight junction protein. Sections were stained with antibodies to WNK4 (red) and ZO-1, (green). The WNK4 signal is shown alone in panel (F), ZO-1 alone in (G), and the two are superimposed in (H). The two proteins colocalize, demonstrating that WNK4 is associated with the tight junctional complex. Bars, 10 μm.

lular junctions in the CCD (Fig. 6, A through E). WNK4 colocalizes with ZO-1, a known tight junction protein (Fig. 6, F through H) but not with vinculin, an adherens junction protein (*14*). Thus, WNK4 is part of the tight junction complex. This finding is intriguing, as the tight junction is known to be the barrier to paracellular ionic flux (*31*) and mutations in components of the tight junction have been shown to alter specific paracellular ionic fluxes (*32*).

In summary, our findings establish that mutations in two members of the WNK family of serine-threonine kinases cause PHAII, with the evidence strongly supporting a genetic gain-of-function mechanism. The clustering of WNK4 mutations in a highly conserved domain suggests that they disrupt an interaction at this site required for the normal regulation of WNK4 function. Both kinases localize to distal nephron segments known to play a key role in the homeostasis of electrolytes altered in PHAII (Web fig. 4) (*21*). In the DCT, salt reabsorption is mediated by the electroneutral Na-Cl cotransporter. In the CD, Na^+ is reabsorbed by the epithelial sodium channel (ENaC), with this electrogenic step providing the electrical driving force for K^+ and H^+ secretion. Because PHAII features an increase in salt reabsorption accompanied by diminished excretion of K^+ and H^+, we infer that these kinases are not simply increasing the activity of ENaC. The action of these kinases may serve to increase transcellular or paracellular chloride conductance in the collecting duct, thereby increasing salt reabsorption and intravascular volume, while concomitantly dissipating the electrical gradient and diminishing K^+ and H^+ secretion. This mechanism is consistent with the Cl^- dependence of PHAII (*5, 6*), and with the existence of paracellular Cl^- flux in the CD (*33*). Another possibility is that the mutant kinases cause constitutive activity of the electroneutral Na-Cl cotransporter in the CD, or a marked increase in its activity in its native site, the DCT. Identification of upstream regulators and downstream targets of these kinases will prove important in understanding the WNK signaling pathway(s).

The broad expression of *WNK1* suggests that it may play a role outside the kidney, in which case missense mutations like those seen in *WNK4* might prove lethal. Alternatively, different WNK1 isoforms might have different functional roles which restrict the types of mutation that can produce the PHAII phenotype. Linkage of PHAII to chromosome 1 in other families (*7*) as well as the absence of mutations in WNK1 and WNK4 in many PHAII kindreds indicate that there must be one or more as yet unidentified PHAII genes.

Like patients with PHAII, many individuals with common, so-called "essential" hypertension have low plasma renin activity and respond well to thiazide diuretics, raising the possibility that variants in *WNK1* and *WNK4* may underlie blood pressure variation in the general population. Indeed, the *WNK4* gene lies only 1 Mb from locus *D17S1299*, the site showing the strongest linkage to blood pressure variation in the Framingham Heart Study population (*34*); this same chromosome segment has suggested linkage to hypertension in two other studies (*35, 36*). It will be of interest to determine whether variants that alter *WNK4* function account for this linkage. Finally, WNK kinases and associated components of their signaling pathway(s) in the kidney may represent new targets for the development of antihypertensive diuretic drugs.

References and Notes

1. A. Mosterd *et al.*, *N. Engl. J. Med.* **340**, 1221 (1999).
2. R. P. Lifton, A. G. Gharavi, D. S. Geller, *Cell* **104**, 545 (2001).
3. W. K. Paver, G. J. Pauline, *Med. J. Aust.* **2**, 305 (1964).
4. R. D. Gordon, S. A. Klemm, T. J. Tunny, M. Stowasser, in *Hypertension: Pathophysiology, Diagnosis, and Management*, J. H. Laragh, B. M. Brenner, Eds. (Raven, New York, 1995), pp. 2111–2123.
5. M. Schambelan, A. Sebastian, F. C. Rector Jr., *Kidney Int.* **19**, 716 (1981).
6. C. Take, K. Ikeda, T. Kurasawa, K. Kurokawa, *N. Engl. J. Med.* **324**, 472 (1991).
7. T. A. Mansfield *et al.*, *Nature Genet.* **16**, 202 (1997).
8. S. Disse-Nicodème *et al.*, *Am. J. Hum. Genet.* **67**, 302 (2000).
9. Members of K22 were classified as affected based on $K^+ > 5.0$ and normal glomerular filtration (seven members), or a prior diagnosis of PHAII with current thiazide diuretic treatment (two members); in addition, a 12-year-old was classified as affected based upon K^+ at the upper limit of normal, elevated blood pressure, suppressed plasma renin activity, hyperchloremia, and reduced bicarbonate level. Kindreds studied included two showing definitive linkage to chromosome 12, one linked to chromosome 17, and 16 that are too small to prove linkage to any chromosome segment. Kindreds in which mutations were identified were Caucasian, ascertained in the United Kingdom (3 kindreds), France (2 kindreds), and Israel (1 kindred). Unrelated control subjects were Caucasians from the United States and Europe. The study was approved by the Yale Human Investigation Committee.
10. A genome scan was performed using 380 polymorphic markers spaced at 10-cM intervals. Lod scores were calculated (*37*) specifying PHAII as an autosomal dominant trait (disease allele frequency of 0.0001, penetrance 99%, phenocopy rate of 0.0001).
11. BLAST searches revealed that *D12S341*, *D12S94*, and *D12S91* are on bacterial artificial chromosome (BAC) clone RPCI11-388A16 (GenBank accession AC004765). Three additional dinucleotide repeats were identified on this BAC and are designated *STS42K*, *STS45K*, and *STS60K* (Web table 1) (*21*). All are polymorphic; observed heterozygosities ranged from 0.30 to 0.60 in caucasians.
12. Genomic DNA was digested with enzyme *Pvu*II and Southern blotting was performed using ^{32}P-labeled probes derived from the BAC clone. Probe 1 shown in Fig. 2A encompasses nucleotides 24593 through

25113 and probe 2 corresponds to nucleotides 78807 through 79341 of BAC clone RPCI11-388A16.
13. Primers near deletion endpoints were used to direct PCR with genomic DNA from kindred members as template (Web table 2) (*21*). Products were fractionated by agarose gel electrophoresis and subjected to DNA sequencing.
14. F. H. Wilson *et al.*, data not shown.
15. The genomic and mRNA structure of *hWNK1* and *hWNK4* was determined by genomic and EST database mining with experimental confirmation (*21*). The cDNA sequence of *hWNK1* has recently been independently submitted to GenBank (NM_018979). The cDNA sequence of *hWNK4* has been deposited in GenBank (AF390018) (Web fig. 1) (*21*).
16. B. Xu *et al.*, *J. Biol. Chem.* **275**, 16795 (2000).
17. Probes spanning exons 5 through 8 of *hWNK1* or exons 16 through 19 of *hWNK4* were hybridized to human multiple-tissue Northern blots (Clontech). Independent blots yield comparable results.
18. Other deletions in intron 1 were sought in unaffected subjects by quantitative PCR and Southern blotting; no deletions that overlap those found in K22 and K4 were identified, although a more proximal 8-kb deletion, unrelated to PHAII, was found to have an allele frequency of 10% in caucasians (*21*).
19. Variants in *WNK1* and *WNK4* were sought using single-strand conformational polymorphism analysis with specific primer pairs (Web table 3) (*21*) directing PCR using genomic DNA as a template. The DNA sequence of identified variants was determined.
20. Levels of gene transcripts were evaluated by real-time quantitative reverse transcription PCR (RT-PCR) using RNA extracted from leukocytes of members of K4 and control subjects (*21*).
21. Supplementary data are available at www.sciencemag.org/cgi/content/full/293/5532/1107/DC1.
22. For *WNK1*, rat sequence is known (*16*) and for *WNK4*, mouse (F. Wilson, unpublished data) and rat sequence (H. Toka, unpublished data) are known from genomic mining and PCR amplification of kidney cDNA.
23. Z. Farfel *et al.*, *Arch. Intern. Med.* **138**, 1828 (1978).
24. Kindred 13 was as previously described with an additional six members characterized since the initial linkage report (*7*); analysis of linkage in the extended kindred yielded a lod score of 5.4, localizing the disease gene to a 16-cM interval flanked by loci *D17S1166* and *D17S931*.
25. The index case of K23 has hypertension, hyperkalemia, distal renal tubular acidosis, suppressed plasma renin activity, and normal glomerular filtration, typical of PHAII.
26. M. R. Lee, S. G. Ball, T. H. Thomas, D. B. Morgan, *Q. J. Med.* **48**, 245 (1979).
27. M. R. Lee, D. B. Morgan, *Lancet* **1**, 879 (1980).
28. M. Baz *et al.*, *Presse Med.* **19**, 1981 (1990).
29. Affinity-purified antibodies to WNK1 and WNK4 were prepared (*21*). Their specificities were established by immunoblotting, demonstrating staining of the immunizing peptide and proteins of appropriate size in mouse kidney (*21*). All staining was competed by the immunizing peptide (*14*).
30. Sections (3 μm thickness) were cut from frozen mouse kidney specimens, fixed, immunostained with indicated antibodies, and subjected to immunofluorescence microscopy. WNK1 and WNK4 staining were both competed by the immunizing peptide (*14*).
31. J. L. Madara, *Annu. Rev. Physiol.* **60**, 143 (1998).
32. D. B. Simon *et al.*, *Science* **285**, 103 (1999).
33. V. L. Schuster, J. B. Stokes, *Am. J. Physiol.* **253**, F203 (1987).
34. D. Levy *et al.*, *Hypertension* **36**, 477 (2000).
35. C. Julier *et al.*, *Hum. Mol. Genet.* **6**, 2077 (1997).
36. J. Baima *et al.*, *Hypertension* **34**, 4 (1999).
37. G. M. Lathrop *et al.*, *Proc. Natl. Acad. Sci. U.S.A.* **81**, 3443 (1984).
38. The left and right ends of the segment shown lie at nucleotide positions 9575 and 107547 on BAC clone accession AC004765 in GenBank.
39. A. Lupas, M. Van Dyke, J. Stock, *Science* **252**, 1162 (1991).
40. Amino acids for WNK2 and WNK3 are numbered with respect to GenBank entries reporting partial sequence for these genes (hWNK2, GenBank accession AB044546; hWNK3, GenBank accession AJ409088).
41. We thank the families studied for their invaluable contribution to this work. Supported in part by an NIH Specialized Center of Research in Hypertension, grants from INSERM and the Association Claude Bernard. S.D-N. is a fellow of the Ministère de l'Education Nationale, de la Recherche et de la Technologie. K.C. is an investigator of the Medical Scientist Training Program. RPL is an investigator of the Howard Hughes Medical Institute.

24 May 2001; accepted 29 June 2001

REPORTS

Resolving the Structure of Ionized Helium in the Intergalactic Medium with the Far Ultraviolet Spectroscopic Explorer

G. A. Kriss,[1,2]* J. M. Shull,[3] W. Oegerle,[4] W. Zheng,[2] A. F. Davidsen,[2]† A. Songaila,[5] J. Tumlinson,[3] L. L. Cowie,[5] J.-M. Deharveng,[6] S. D. Friedman,[2] M. L. Giroux,[3] R. F. Green,[7] J. B. Hutchings,[8] E. B. Jenkins,[9] J. W. Kruk,[2] H. W. Moos,[2] D. C. Morton,[8] K. R. Sembach,[2] T. M. Tripp[9]

The neutral hydrogen (H I) and ionized helium (He II) absorption in the spectra of quasars are unique probes of structure in the early universe. We present Far-Ultraviolet Spectroscopic Explorer observations of the line of sight to the quasar HE2347-4342 in the 1000 to 1187 angstrom band at a resolving power of 15,000. We resolve the He II Lyman α (Lyα) absorption as a discrete forest of absorption lines in the redshift range 2.3 to 2.7. About 50 percent of these features have H I counterparts with column densities $N_{H\ I} > 10^{12.3}$ per square centimeter that account for most of the observed opacity in He II Lyα. The He II to H I column density ratio ranges from 1 to >1000, with an average of ~80. Ratios of <100 are consistent with photoionization of the absorbing gas by a hard ionizing spectrum resulting from the integrated light of quasars, but ratios of >100 in many locations indicate additional contributions from starburst galaxies or heavily filtered quasar radiation. The presence of He II Lyα absorbers with no H I counterparts indicates that structure is present even in low-density regions, consistent with theoretical predictions of structure formation through gravitational instability.

The intergalactic medium (IGM) is the gaseous reservoir that provides the raw material for the galaxies that dominate our view of the visible universe. By observing distant bright objects such as quasars, we can explore the IGM by examining the absorption features it imprints on the transmitted light. These absorption features trace structure in the universe at epochs intermediate between the earliest density fluctuations seen in the cosmic background radiation and the distribution of galaxies visible today. The distribution of absorption features according to redshift (z) and the column densities of gaseous material in different ions reveal the structure of the IGM and its density and ionization state. From the ionization state of the gaseous species, we can also infer the processes responsible for ionizing the gas (e.g., radiation from quasars in the early universe or from early bursts of star formation).

The lack of smooth Lyα absorption by H

[1]Space Telescope Science Institute, 3700 San Martin Drive, Baltimore, MD 21218, USA. [2]Center for Astrophysical Sciences, Department of Physics and Astronomy, Johns Hopkins University, Baltimore, MD 21218, USA. [3]CASA and JILA, Department of Astrophysical and Planetary Sciences, University of Colorado, Campus Box 389, Boulder, CO 80309, USA. [4]Laboratory for Astronomy and Solar Physics, Code 681, NASA/Goddard Space Flight Center, Greenbelt, MD 20771, USA. [5]Institute for Astronomy, University of Hawaii, 2680 Woodlawn Road, Honolulu, HI 96822, USA. [6]Laboratorie d'Astronomie Spatiale, BP 8, 13376 Marseille Cedex 12, France. [7]Kitt Peak National Observatory, National Optical Astronomy Observatories, Post Office Box 26732, 950 North Cherry Avenue, Tucson, AZ 85726, USA. [8]Herzberg Institute of Astrophysics, National Research Council of Canada, Victoria, BC V8X 4M6, Canada. [9]Princeton University Observatory, Princeton, NJ 08544, USA.

*To whom correspondence should be addressed. E-mail: gak@stsci.edu
†Deceased.